TOPICAL REVIEW — Magnetism, magnetic materials, and interdisciplinary research

Perpendicular magnetic tunnel junction and its application in magnetic random access memory*

Liu Hou-Fang(刘厚方), Syed Shahbaz Ali, and Han Xiu-Feng(韩秀峰)†

Beijing National Laboratory of Condensed Matter Physics, Institute of Physics, Chinese Academy of Sciences, Beijing 100190, *China*

(Received 23 April 2014; published online 13 June 2014)

Recent progresses in magnetic tunnel junctions with perpendicular magnetic anisotropy (PMA) are reviewed and summarized. At first, the concept and source of perpendicular magnetic anisotropy (PMA) are introduced. Next, a historical overview of PMA materials as magnetic electrodes, such as the RE–TM alloys TbFeCo and GdFeCo, novel tetragonal manganese alloys Mn–Ga, $L1_0$-ordered (Co, Fe)/Pt alloy, multilayer film $[Co, Fe, CoFe/Pt, Pd, Ni, Au]_N$, and ultra-thin magnetic metal/oxidized barrier is offered. The other part of the article focuses on the optimization and fabrication of CoFeB/MgO/CoFeB p-MTJs, which is thought to have high potential to meet the main demands for non-volatile magnetic random access memory.

Keywords: magnetic random access memory, perpendicular magnetic anisotropy, spin transfer torque effect, magnetic tunnel junction

PACS: 75.30.Gw, 75.50.Ss, 75.76.+j, 85.75.Dd **DOI:** 10.1088/1674-1056/23/7/077501

1. Introduction

Compared with other random access memory (such as SRAM, DRAM, non-flash), magnetic random access memory (MRAM) has attracted considerable interest as a fast, low-power consumption, long-service-life, radiation-resistant, and non-volatile memory.[1–6] The first generation of MRAM utilized the Oersted field induced by current in adjacent conducting lines to switch the magnetization of a free layer. However, in such a device, when the size of the memory cell is reduced below 0.1 μm, the writing power must increase rapidly because the switching current is inversely proportional to the cell size. Meanwhile the long-term stability of the memory cell would also be jeopardized due to thermal activation induced by the high power.[7]

In 1996, Slonczewski and Berger predicted that spin-polarized current could reversibly switch the magnetization of a ferromagnetic layer — an effect called spin-transfer torque (STT).[8,9] In 2000, Katine *et al.* were the first to realize SST by using spin-polarized current to switch the magnetization of a Co layer in a Co/Cu/Co nano-pillar with diameter about 100 nm.[10] Subsequently, a number of research groups demonstrated the effect in ferromagnetic layers in amorphous AlO_x- or crystalline MgO-based nano-size MTJs.[11–13] With the improvement of nano-fabrication and ultra-thin film deposition technology, MRAM with switching via STT effect, which is generally called STT-MRAM, has become a strong candidate for future memory applications.

Until now, the critical tasks in developing STT-MRAM for future non-volatile memory lie in finding ways to reduce the switching current density J_c and validate that the STT switching characteristics are sustainable under the same circumstances where the conventional field-driven MRAM is expected to meet serious scaling problems.[14]

For in-plane MTJs, the intrinsic current density is given by[15,16]

$$\text{In-plane}: I_C = \left(\frac{2e}{\hbar}\right)\frac{2\alpha}{g(\boldsymbol{m}\cdot\boldsymbol{p})p}(U_K + \pi M_s^2). \tag{1}$$

However, for the perpendicular-anisotropy MTJs (p-MTJs) case, the intrinsic current density is given by[15,16]

$$\text{Out-of-plane}: I_C = \left(\frac{2e}{\hbar}\right)\frac{2\alpha}{g(\boldsymbol{m}\cdot\boldsymbol{p})p}(U_k), \tag{2}$$

where M_s, U_k, and α are the saturation magnetization, the energy barrier and the damping constant. Therefore, from Eqs. (1) and (2), the switching current for MTJs with perpendicular anisotropy is lower than that of in-plane MTJs. Moreover, smaller J_c is good for reducing the size of the transistor and achieving denser storage. The thermal stability can be defined as the thermal factor $\Delta = U_k/k_BT = H_{eff}M_sV/2$, where H_{eff} is the effective anisotropy field, and M_s and V are the volume and saturation magnetization of the free layer, respectively. For p-MTJs, the thermal factor Δ can be improved by using high magnetic anisotropy materials without sacrificing the low current density. Therefore, these PMA materials can be explored as the electrodes for magnetic tunnel junctions (MTJs).

*Project supported by the State Key Project of Fundamental Research of Ministry of Science and Technology, China (Grant No. 2010CB934400) and the National Natural Science Foundation of China (Grant Nos. 51229101 and 11374351).

†Corresponding author. E-mail: xfhan@iphy.ac.cn

© 2014 Chinese Physical Society and IOP Publishing Ltd

In the following sections, first we will introduce the concept and source for the perpendicular magnetic anisotropy (PMA), and then discuss several kinds of PMA materials, such as rare-earth/transition metal (RE–TM) alloys TbFeCo and GdFeCo,[17] novel tetragonal manganese alloys Mn–Ga,[18,19] $L1_0$-ordered (Co, Fe)/Pt alloy,[20,21] multilayer film based on [Co, Fe, CoFe/Pt, Pd, Ni, Au] with a number of periods,[22–24] and ultra-thin magnetic metal/oxidized barrier.[25] Later, the optimization and fabrication of PMA CoFeB/MgO system will be addressed.

2. Perpendicular magnetic anisotropy (PMA)

Magnetic anisotropy is the energy required to switch the easy-axis magnetization to the hard-axis magnetization, which can be formed by electric field, interface, stress or shape of a solid or crystal. There are several sources for magnetic anisotropy: (I) magneto-crystalline anisotropy, (II) magneto-elastic anisotropy, (III) shape anisotropy. The effective magnetic anisotropy field is denoted as $H_{\rm ani}$, with direction usually parallel to the easy-axis.[26] For uniaxial magnetic anisotropy, the effective magnetic anisotropy field can be expressed as

$$H_{\rm ani} = \frac{2K_1}{M}\cos\gamma, \tag{3}$$

in which γ is the angle between the easy axis and the magnetization, and K_1 is the anisotropy constant. The magnetic anisotropy energy $E_{\rm ani}$ has the form:

$$E_{\rm ani} = K_1\sin^2\gamma + K_2\sin^4\gamma + K_3\sin^6\gamma + \cdots, \tag{4}$$

where for example, K_1 is larger than other parts in a thin film, and γ is defined as the angle between the normal direction and the magnetization direction. The anisotropy constant could be separated as a crystalline anisotropy $K_{\rm u}$ and shape anisotropy $K_{\rm s}$. If $(K_{\rm u}+K_{\rm s})>0$, the multilayer film favors perpendicular magnetization, while for $(K_{\rm u}+K_{\rm s})<0$, the film is prone to in-plane magnetization. Considering the interfacial anisotropy $K_{\rm i}$, the effective magnetic anisotropy could be written as

$$K_{\rm u} = K_{\rm b} - M_{\rm s}^2/2\mu_0 + K_{\rm i}/t, \tag{5}$$

where $K_{\rm b}$ is the bulk crystalline anisotropy, which is typically negligible, $K_{\rm i}$ is the interfacial anisotropy, and t is the thickness of the thin film. The values of $K_{\rm b}$ and $K_{\rm i}$ can be obtained by fitting the relation between the product $K_{\rm u}t$ and t. Figure 1 shows the fitting results for Co/Pd multilayer.[27] According to the Eq. (5), the intercept $K_{\rm i}>0$ indicates that the direction of magnetization prefers perpendicular alignment to the layer plane. The slope $(K_{\rm b}-M_{\rm s}^2/2\mu_0)<0$ means that the magnetization favors in-plane alignment. In other words, at a certain thickness $t_\perp$ (here 13 Å), the contribution of bulk magnetization anisotropy is equal to interfacial anisotropy.

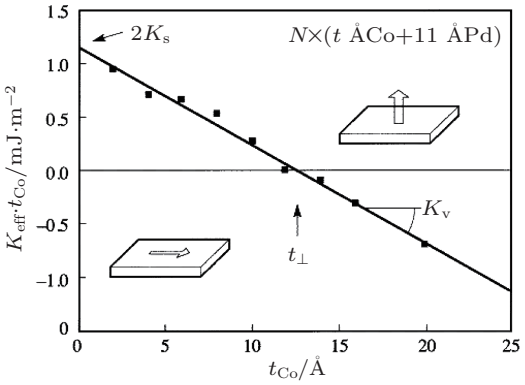


Fig. 1. The product $K_{\rm eff}\cdot t$ versus the thickness t for Co/Pd multilayer films. The vertical axis intercept equals the interface anisotropy, whereas the slope of linear data gives the bulk anisotropy contribution.[27]

3. Perpendicular magnetic anisotropy materials

There are several kinds of perpendicular magnetic anisotropy (PMA) materials. Multilayer films based on transition metal (TM) like Co, Fe, CoFe, and noble metal such as Pt, Pd, Ni, and Au with number of periods, exhibit perpendicular magnetic anisotropy (PMA), which is mainly attributable to the interfacial anisotropy rather than the magnetocrystalline anisotropy. The interfacial anisotropy can be several orders magnitude larger than the magnetocrystalline anisotropy, especially with a smooth interface between the TM and the noble metal. The magnetic properties of these multilayer films can be easily modified by changing the number of periods or the thickness of the TM or the noble metal.

In the other case of rare-earth/transition metal (RE–TM) alloys TbFeCo and GdFeCo, the mechanism of perpendicular magnetic anisotropy has not yet been fully understood. Several mechanisms such as anisotropic chemical bonding of Fe 3d and Tb 4f electrons, exchange anisotropy, and anti-parallel dipole have been considered to explain the origin of the perpendicular anisotropy. On the other hand, $L1_0$-ordered (Co, Fe)/Pt alloys show very high perpendicular anisotropy due to magnetocrystalline anisotropy from hybridization between the Pt 5d band and Co or Fe 3d band electronic states. The key challenge in achieving high perpendicular anisotropy for these materials is the fabrication of perfect texture by using suitable underlayer and annealing temperature.

Recently, novel tetragonal manganese alloys $Mn_{3-\delta}Ga$ with large perpendicular anisotropy ($K_{\rm u}\sim 1$–2×10^7 erg/cm^3), a high predicted spin polarization value of 70%–88%, small damping constant α ($\alpha<0.008$), low saturation magnetization and Curie temperature of 730–770 K depending on δ[28,29] were also reported. These materials have the potential to be excellent candidates for spintronics materials. However, a large lattice mismatch exists in the MnGa and MgO tunnel barrier, resulting very low TMR ratio. The insertion of a conventional 3d transition metal layer, such as Co, Fe, and CoFeB, between the MnGa electrode and the

MgO tunnel barrier is always used to overcome the mismatch problem. Figures 2(a) and 2(b) show the unit cell of $L1_0$-Mn_xGa ($1 < x < 1.8$) and cross-sectional TEM image of MTJ with a stack structure of $L1_0$–$Mn_{62}Ga_{38}$(30)/Fe(1.1)/Mg(0.4)/MgO(2)/$Co_{50}Fe_{50}$/Cap layer.

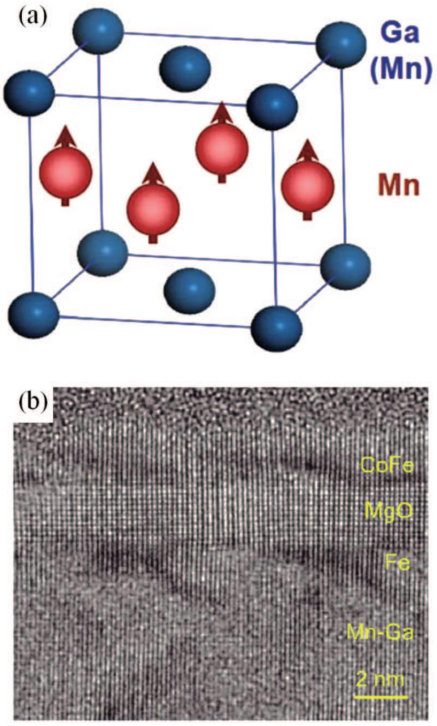


Fig. 2. (a) Unit cell of $L1_0$-Mn_xGa ($1 < x < 1.8$), (b) cross-sectional TEM image of MTJ with stack structure of $L1_0$–$Mn_{62}Ga_{38}$(30)/Fe(1.1)/Mg(0.4)/MgO(2)/$Co_{50}Fe_{50}$/Cap layer.[29]

In addition, according to first-principles calculations, ultra-thin magnetic metal/oxidized barrier[30–32] shows perpendicular anisotropy, due to PMA interfacial contribution from hybridization between the Fe 3d band and O 2p orbitals (Fig. 3(a)), elastic stress due to the lattice distortion (Fig. 3(b)), and crystal symmetry breaking down due to the interface (Fig. 3(c)). An ultra-thin Fe, CoFeB, and CoFeAl/MgO barrier with PMA has also been demonstrated ($K_u \sim 10^6$ erg/cm^3). Today, these materials are thought of as the well-known body centered cubic (bcc) material systems that are good for a high TMR ratio in MTJs.[33]

Compared with the in-plane anisotropy electrodes, PMA materials have following advantages: (i) avoiding the edge effect. For deep submicron patterned magnetic film, use of PMA materials can avoid magnetization curling, which is usually due to edge domain configurations and is always observed for in-plane materials; (ii) reducing the feature size. In-plane MTJs usually have lower effective magnetic anisotropy than PMA MTJs (p-MTJs), so the critical size of in-plane MTJs is larger than that of p-MTJs, due to a superparamagnetism effect. When storage density is up to Tbit/in^2, the dimension of a memory cell is tens of nanometers or even smaller.[34] Therefore, p-MTJs with smaller feature size not only increase the storage density but also meet the demand for thermal stability; (iii) lowering the switching current density. According to recent progress in semiconductor technology, the switching current density for the MTJ as a memory cell should be further reduced to allow lower-power operation.

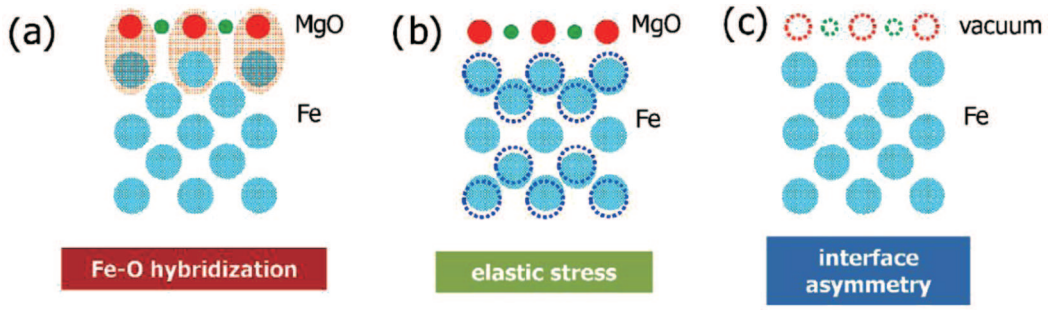


Fig. 3. Schematic of main contribution to the PMA Fe–MgO system.[33] (a) Fe–O hybridization; (b) elastic stress; (c) interface asymmetry.

Researchers from industrial firms and research institutes try to discover, optimize and utilize PMA electrode materials for MTJs, which is a very promising research field. In 2002, Nishimura *et al.* measured the TMR ratio of 55% in GdFeCo/CoFe/AlO_x/CoFe/TdFeCo p-MTJs at room temperature (RT), shown in Fig. 4.[35] In 2007, a TMR ratio of 74% was obtained in double barrier p-MTJ with GdFeCo/AlO_x/GdFeCo/FeCo/AlO_x/FeCo/TbFeCo stack structure by Cabrera *et al.*[36]

In 2008, Nakayama *et al.* studied spin-transfer switching in the TbCoFe/CoFeB /MgO/CoFeB/TbCoFe MTJ with a TMR ratio about 15%, current density of 4.7 MA/cm^2 and thermal stability factor of 107 at RT, shown in Fig. 5.[37] In the same year, Park *et al.* observed TMR ratio of 15% at RT in Co/Pt multilayer electrodes and AlO_x barrier.[38] Due to the spin filter effect of the MgO tunnel barrier, Ye *et al.* investigated the effect of annealing on $[Co/Pd]_{10}$/MgO/$[Co/Pt]_5$ p-MTJ, and obtained the TMR ratio of 32% by insertion of

Mg layers on both sides of the MgO barrier.[39] Unfortunately, Co/Pt and Co/Pd multilayers with fcc (111) structure mismatch with the texture of bcc MgO (001).

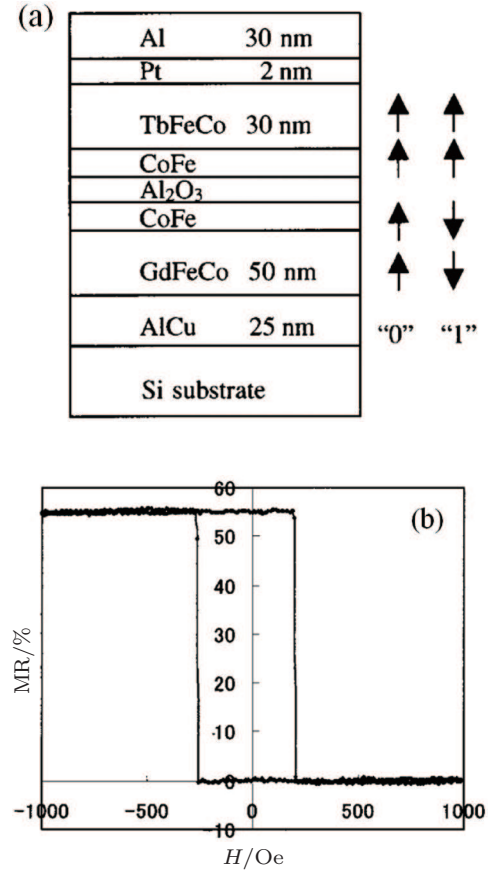


Fig. 4. (a) Schematic of GdFeCo(50)/CoFe(1)/Al-O(2.2)/CoFe(1)/TbFeCo p-MTJs structure and (b) TMR ratio curve measured at RT.[35]

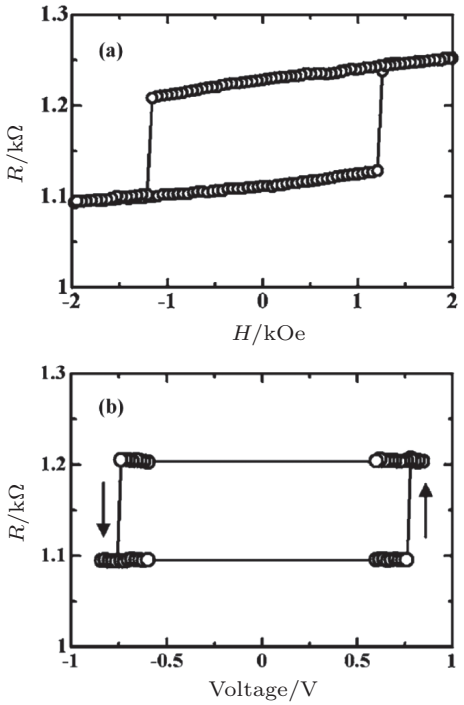


Fig. 5. (a) *R–H* and (b) spin-transfer switching curves of the TbFeCo(30)/CoFeB(2)/MgO(1) /CoFeB(1)/TbFeCo(3 nm) MTJ stack structure.[37]

High TMR ratio and low resistance–area (RA) product are the key points for developing ultra-high density MRAM. In 2010, Yakushiji *et al.* succeeded in patterning the MgO-based MTJs with $[Co/Pt]_n$/CoFeB/CoFe as a free layer and CoFe/CoFeB/TbFeCo as a reference layer. After annealing at relatively low temperature of 225 °C, they obtained TMR ratio of up to 85% at RT and a low resistance-area (RA) product of 4.4 $\Omega \cdot \mu m^2$. With post-annealing temperature increasing $T_a > 225$ °C, TMR ratio decreases rapidly, due to the crystallization of CoFeB layer adjacent [Co/Pt] superlattice into fcc (111) orientation, shown in Fig. 6.[40] In 2011, Mizunuma *et al.* investigated the TMR ratio of 101% after annealing at 300 °C in the $[CoFe/Pd]_N/Co_{20}Fe_{60}B_{20}$/MgO (2 nm)/$Co_{20}Fe_{60}B_{20}$/$[Pd/CoFe]_{10}$ p-MTJ with two different Pd layer thicknesses. By reducing the B composition in the CoFeB layer, they obtained the high TMR ratio of 120%.[41,42] However, the damping constant α is several times larger than the regular FM layer because of the strong spin–orbit interaction of Pt or Pd, leading to a large switching current density, according to Eqs. (4) and (5). Novel perpendicular magnetic anisotropy materials should be optimized to meet the demand for a high perpendicular anisotropy energy K_u, a low damping constant and a high TMR ratio.

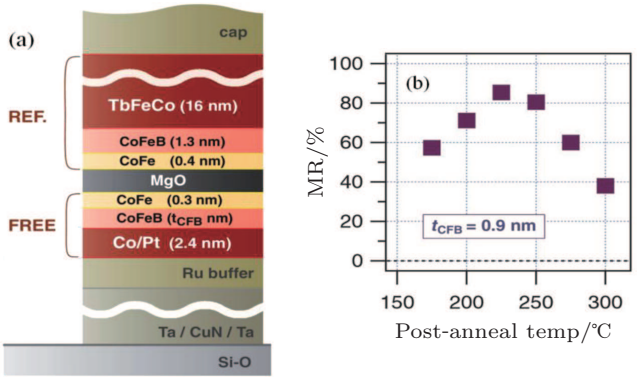


Fig. 6. (a) Schematic of [Co/Pt] (2.4)/CoFeB(t)/CoFe (0.3)/MgO/CoFe (0.4)/CoFeB (1.3)/ TbFeCo (16 nm) p-MTJs structure, (b) MR ratio versus post-annealing temperature.[40]

In 2010, Ikeda *et al.* realized PMA in Ta/CoFeB/MgO/CoFeB/Ta MTJs with the thickness of the CoFeB layers being less than 1.5 nm. The perpendicular anisotropy energy density K_u is up to 2.1×10^6 erg/cm^3 at $t_{CoFeB} = 1.3$ nm, and increases as the thickness of the CoFeB layer is reduced. The damping constant α was less than 0.03, as determined from the FMR spectra. A TMR ratio of over 120% and RA = 18 $\Omega \cdot \mu m^2$ were achieved in 40-nm-scale Ta/$Co_{20}Fe_{60}B_{20}$(1.0)/MgO(0.85)/$Co_{20}Fe_{60}B_{20}$(1.7 nm)/Ta p-MTJ after annealed at 300 °C. In addition, switching current density J_{c0} and thermal stability factor E/k_BT were 3.9×10^6 A/cm^3 and 43, respectively. Figure 7 shows the schematic structure of CoFeB-MgO p-MTJs, magnetic properties of single CoFeB layer and *R–H* (*I*) curves.[43] These results demon-

strate that CoFeB-MgO system is capable of supporting the low J_{c0}, sufficient thermal stability E/k_BT and high TMR ratio, which was a breakthrough for high-density memories and logic circuits.

Table 1 summarizes the publications on p-MTJs. Until now, the TMR ratio of over 120% at RT in CoFeB/MgO/CoFeB system was by far the highest among these kinds of p-MTJs. Recently, current-induced magnetization switching was successfully demonstrated in Ta/CoFeB/MgO/CoFeB/Ta p-MTJs with the smallest feature size of 17 nm, for investigating the downscaling feasibility of STT-MRAM.[44]

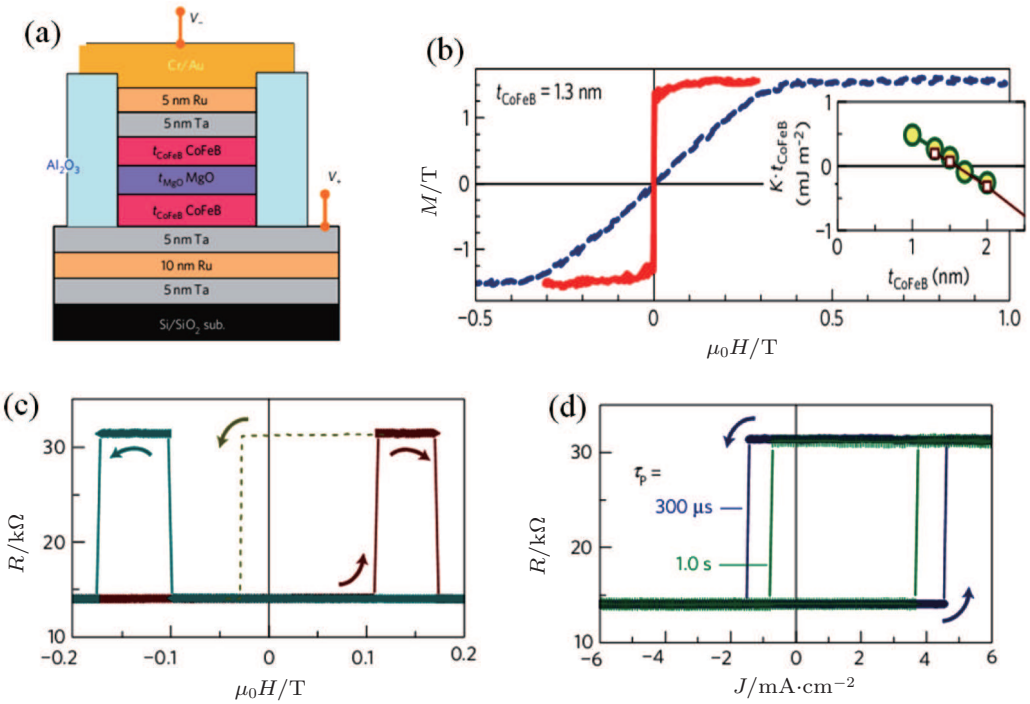


Fig. 7. (a) Schematic structure of CoFeB-MgO p-MTJs, (b) magnetic properties of single CoFeB layer, and (c) perpendicular *R–H* curve and (d) current-induced-magnetization-switching loop at current pulse duration of 300 μs and 1 s.[43]

Table 1. Publications on p-MTJs.

No.	Core structure/nm	TMR/%	Ref.
1	GdFeCo(50)/CoFe(1)/Al-O(2.2)/CoFe(1)/TbFeCo	55	2002 *J. Appl. Phys.* **91** 5246
2	GdFeCo/AlO_x/GdFeCo/FeCo/AlO_x/FeCo/TbFeCo	74	2007 *IEEE Trans. Magn.* **43** 914
3	TbFeCo/CoFeB(2)/MgO(1)/CoFeB(1)/ TbFeCo(3)	15	2008 *J. Appl. Phys.* **103** 07A710
4	GdFeCo(100)/Fe(3)/MgO(2)/Fe(3)/TbFeCo(100)	64	2008 *J. Appl. Phys.* **103** 07A911
5	L1-CoPt(20)/MgO(3)/L1-CoPt(30)	6	2008 *Appl. Phys. Lett.* **92** 172502
6	L1-FePt(3)/MgO/Fe(2)/L1-FePt	120	2008 *IEEE Trans. Magn.* **44** 11
7	$[CoFe/Pd]_3$/CoFeB/MgO/Fe/$[Pd/CoFe]_{10}$	78	2009 *Appl. Phys. Lett.* **95** 232516
8	Ta/CoFeB/MgO/CoFeB/$[Co/Pd]_4$	41	2009 *Appl. Phys. Lett.* **98** 022501
9	$[Co/Pt]_6$/Co(0.5)/Al-O /$[Co/Pt]_3$	14.7	2010 *J. Appl. Phys.* **107** 09C711
10	[CoFe(0.2)/Pd(1.2)]$_3$/CoFeB(3)/MgO(2)/CoFeB(3) /$[CoFe(0.2)/Pd(1.2)]_{10}$	91	2010 *Jpn. J. Appl. Phys.* **49** 04DM04
11	[Co(0.24)/Pt(0.16)]/CoFeB(1.1)/CoFe(0.30)/MgO(1.1) /CoFe(0.4)/CoFeB(1.3)/TbFeCo(16)	85	2010 *Appl. Phys. Exp.* **3** 053003
12	CoFeB(1.3)/MgO(0.85)/CoFeB(1.3)	124	2010 *Nat. Mater.* **9** 721
13	$[CoFe/Pd]_N$/CoFeB/MgO(2)/ CoFeB/$[Pd/CoFe]_{10}$	120	2011 *J. Appl. Phys.* **109** 07C711
14	Cr/MnGa(30)/Mg(0.4)/MgO(2.2)/CoFe(2.5)	23@10 K	2011 *Appl. Phys. Lett.* **99** 192509
15	MnGa/Co/Mg(0.4)/MgO(1.8)/CoFeB(1.2)	40	2012 *Appl. Phys. Lett.* **101** 032402
16	CoFeAl/MgO/(CoFe, Fe)/CoFeB	91	2012 *Appl. Phys. Exp.* **5** 063003

4. Optimization and fabrication of CoFeB/MgO/CoFeB p-MTJs

4.1. Perpendicular magnetic anisotropy in CoFeB/MgO stack layer

In order to systematically study the magnetic and magneto-electric transport properties of CoFeB/MgO p-MTJs, Wang *et al.*[45] were first to prepare the multilayer structures of Ta(5)/Ru(10)/Ta(5)/CoFeB(t_1:0.6–1.8)/ MgO(2.5) and Ta(5)/MgO(2.5)/CoFeB(t_2:0.6–2.2)/Ta(5 nm) on thermally oxidized silicon by magnetron sputtering, and then post annealed the samples at different temperatures in vacuum for 1 h. They investigated an increase in PMA with an increase in the

annealing temperature up to 350 °C. When the annealing temperature was higher than 350 °C, both H_c and K_u were reduced due to the intermixing of CoFeB and Ta at their interface. The phase diagrams of perpendicular anisotropy with annealing temperature and thickness of CoFeB layer in Ta/CoFeB/MgO and MgO/CoFeB/Ta were summarized from experimental data points, as shown in Fig. 8.[45]

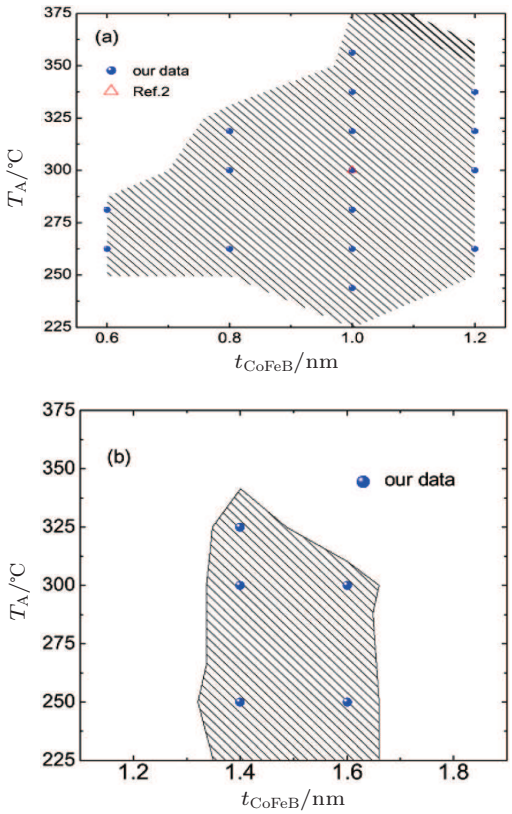


Fig. 8. The phase diagram: annealing temperature and thickness of CoFeB layer dependence of out-of-plane Mr/Ms in Ta/CoFeB/MgO (a) and in MgO/CoFeB/Ta.[45]

4.2. TMR effect and magneto-electric properties in CoFeB/MgO/CoFeB p-MTJ

According the phase diagram of PMA, the multilayer of Ta(5)/Ru(10)/Ta(5)/ CoFeB (1.2)/MgO(2)/CoFeB (1.4)/Ta(5)/Ru (6 nm) was deposited by the sputtering system. Junctions with 5×10 μm^2 were fabricated by microfabrication technique, and then annealed at 300 °C in vacuum to obtain high TMR ratio with good PMA. The magnetic and transport properties were measured in SQUID and PPMS systems respectively. Figure 9(a) shows the out-of-plane magnetization versus the magnetic field M–H loop at 2 K for the CoFeB(1.2)/MgO(2)/CoFeB(1.4 nm) stack film annealed at 300 °C. The coercivity H_c of top CoFeB is larger than that of bottom CoFeB, so the magnetization of bottom CoFeB layer switches first during the magnetic field changes from positive to negative. From TMR–H curve shown in Fig. 9(b), switching between parallel (P) and antiparallel (AP) configurations was clearly separated, and the out-of-plane TMR ratio was about 128% at 300 K.

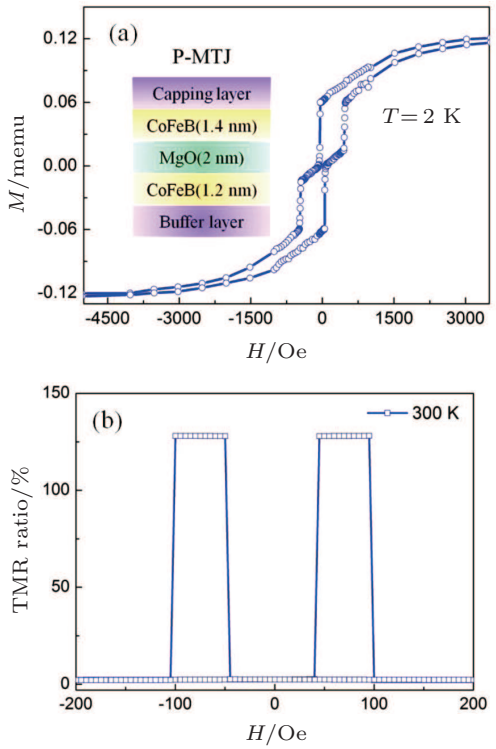


Fig. 9. (a) Out-of-plane magnetization versus magnetic field M–H loop at 2 K for the CoFeB(1.2)/MgO(2)/CoFeB(1.4 nm); inset: schematic of PMA CoFeB/MgO/CoFeB film structure. (b) TMR curve for the MTJ device after annealing treatment.

For an in-plane, PMA MTJ device, the tunneling transport properties usually include the elastic and the inelastic tunneling modes. The elastic tunneling mode means that spin-polarized electrons during tunneling process do not lose energy. In fact, the spin-polarized electrons will interact with magnetic impurities at the FM electrode/barrier interface, defects in the barrier and the crystal lattice of FM electrodes and barrier, and result in excitation of magnon and phonon, which can be studied by inelastic electron-tunneling spectroscopy (IETS, $\mathrm{d}^2I/\mathrm{d}V^2$).[46] Using this method, sorts of elementary excitations in inelastic scattering process can, in principle, be detected, which are thought as important reasons for decreasing the TMR ratio with high bias voltage.

The dynamic conductance G ($\mathrm{d}I/\mathrm{d}V$) and IETS ($\mathrm{d}^2I/\mathrm{d}V^2$) of the P configuration at 2 K in PMA CoFeB/MgO/CoFeB MTJs are presented in Fig. 10(a), where several multiple peaks in the $\mathrm{d}^2I/\mathrm{d}V^2$ of the P configuration can be seen, in accordance with the electron–magnon and electron–phonon scattering processes. A strong asymmetry in the $\mathrm{d}I/\mathrm{d}V$ curve between positive and negative biases is observed. Such asymmetry has been reported previously by some groups,[47,48] which is usually attributed to different electronic structures of the top and bottom CoFeB/MgO interfaces. The first peak of a zero-bias (ZB) anomaly is clearly visible in IETS (marked ZB in the figure), which is located at

about ±3.8 mV. The ZB anomaly peak is attributed to magnetic impurities and is not dependent on the magnetic configuration of external field.[49,50] The next peak (marked by M) appeared at ±30 mV, which corresponds to the magnon excitation at the FM electrode/barrier interfaces.[51] The M peak is thought to contribute greatly to the TMR behavior during post annealing. The MgO barrier phonon peak (marked by P) is at about 76 mV, typical to MgO-based MTJ.[52] Figure 10(b) shows the temperature dependence on IETS of the P configuration. The M and ZB peak gradually disappear with increasing temperature. At 300 K, only the MgO barrier phonon peak can be visible.

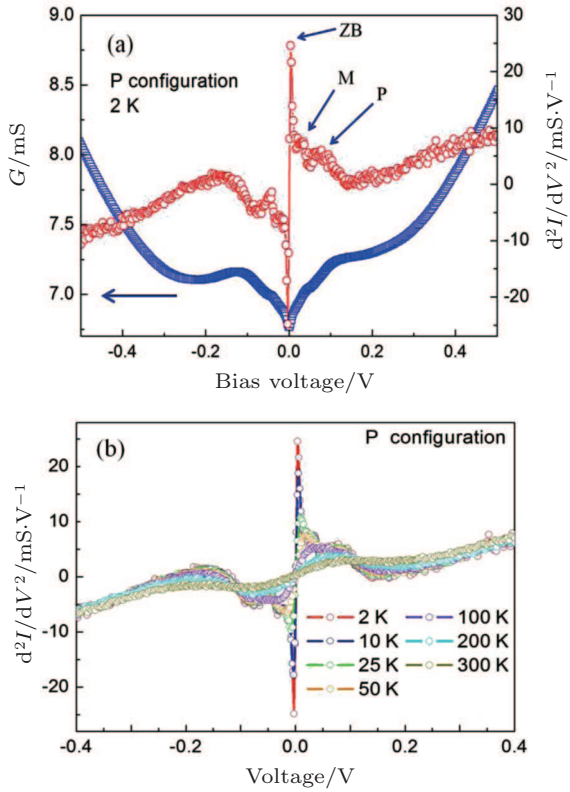


Fig. 10. (a) Dynamic conductance G ($\mathrm{d}I/\mathrm{d}V$) and IETS ($\mathrm{d}^2I/\mathrm{d}V^2$) of the P configuration for PMA CoFeB/MgO/CoFeB MTJ at 2 K; (b) IETS of P configuration versus temperature.

4.3. Electric-field and spin-transfer-torque effect on CoFeB/MgO/CoFeB p-MTJ

Recently, electric-field-induced modification of magnetism in 3d ferromagnets has been investigated by Brillouin light scattering, Kerr effect, ferromagnetic resonance, and anomalous Hall effect. In 2007, Weisheit *et al.*[53] demonstrated that the magnetocrystalline anisotropy of FePt or FePd can be modified by and electric field when it is immersed in an electrolyte, shown in Fig. 11. Although the coercivity of the FePt and FePd thin films were altered by up to 4% and 1%, this experiment confirmed that electric field can modify magnetism of 3d ferromagnets, and it stimulated the emergence of a series of research with interesting results.

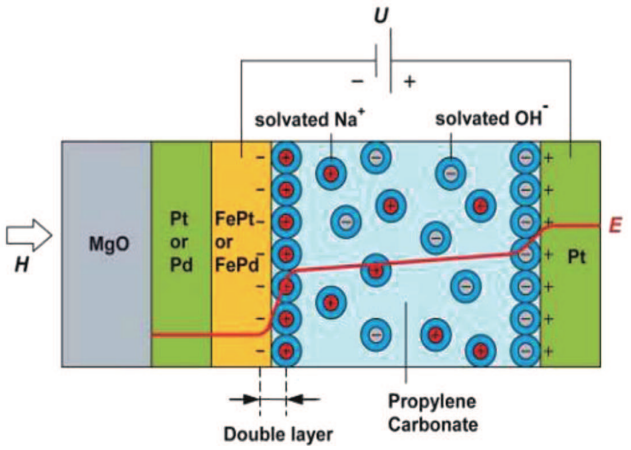


Fig. 11. Schematic of electric-field-induced modification of perpendicular magnetic anisotropy of FePt or FePd in electrolyte propylene carbonate.[53]

Subsequently, in 2009 Maruyama *et al.*[54] utilized the relatively small electric-field causing a large change of about 40% in the magnetic anisotropy of Fe/MgO junctions. However, the resistance switching induced by electric-field had not been realized until perpendicular anisotropy induced by interfacial magnetic anisotropy was demonstrated in magnetic tunnel junctions by Ikeda *et al.* in 2010, because the external electric field can only penetrate into a ferromagnetic electrode by a few monolayers owing to the effect of screening by free electrons.

In pursuit of PMA originating from interfacial magnetic anisotropy at CoFeB/MgO interface, in 2011 Wang *et al.* successfully achieved voltage-induced resistance switching because the electric field can significantly change the interfacial magnetic anisotropy in Ta/CoFeB(1.2–1.3)/MgO(1.2-2)/CoFeB(1.6 nm) p-MTJ. They found that H_c depends quasi-linearly on a bias electric field for the bottom CoFeB electrode, and the top electrode exhibits the opposite dependence, where H_c increases with increasing electric field, as shown in Fig. 12(b). Moreover, they achieved fully reversible unipolar switching of resistance by a series of consecutive negative pulses with alternating amplitudes of −0.9 V and −1.5 V under a constant H_{bias} of 55 Oe, as shown in Figs. 12(c)–12(d). The magnetization state of PMA CoFeB/MgO/CoFeB MTJ was first reset to the antiparallel state under a constant bias field H_{bias}. With the negative bias voltage V_1, the MTJ was switched from P to AP by the STT effect. The switching current density was only about the order of 10^4 A/cm^2 due to PMA and energy barrier U_k reduced by electric field. AP state of MTJ stayed stable after the bias voltage V_1 was removed. The more negative voltage V_2 ($|V_2| > |V_1|$), caused a further reduction of PMA and energy barrier height such that the MTJ state was returned to the P state by the bias field H_{bias}. As the energy barrier height U_k is reduced by applied electric field, the average current density was of the order of 10^4 A/cm^2, demonstrating a good energy-efficient switching process in Fig. 12(e).[55]

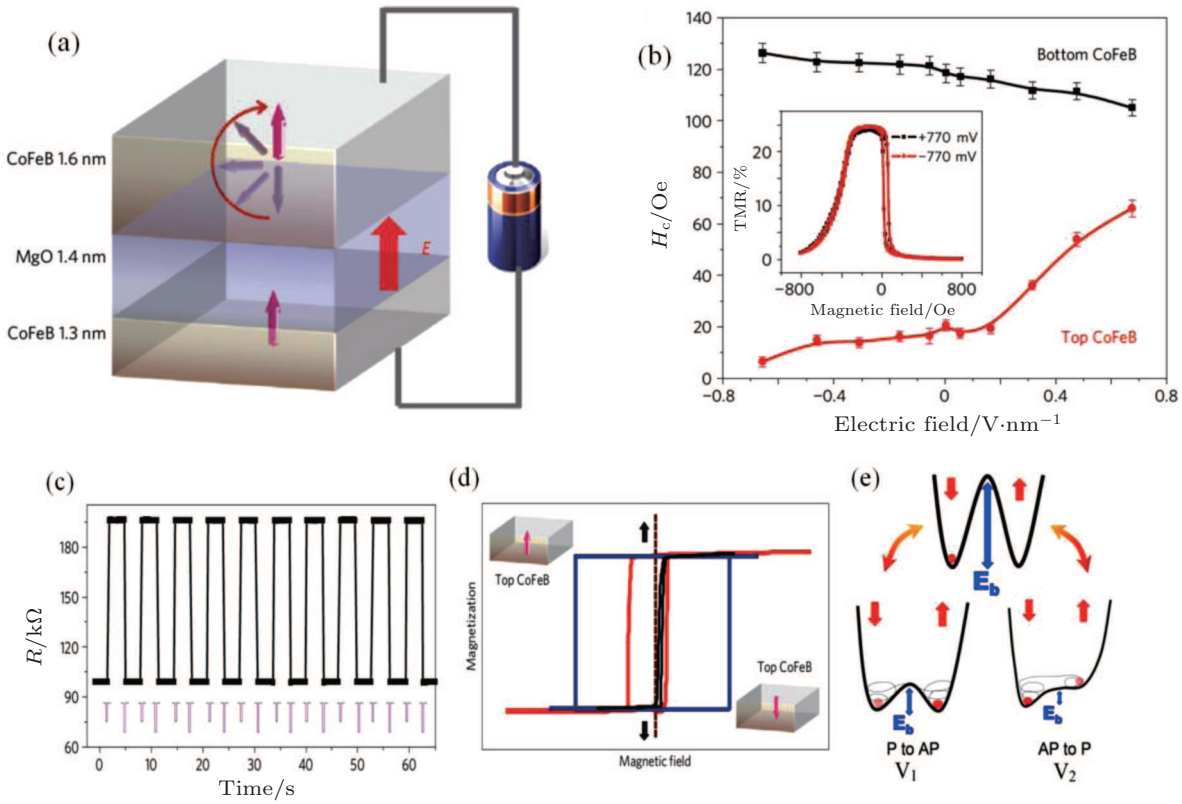


Fig. 12. (a) Schematic drawing of a p-MTJ and the effect of electric field through a small voltage supplied by a battery. (b) Dependence of the coercivities for the top and bottom CoFeB layers on electric field. Error bars designate the s.d. Inset: the TMR curves of an in-plane MTJ under opposite bias voltages. (c) Unipolar switching of the p-MTJ by a series of negative pulses with alternating amplitudes of −0.9 V and −1.5 V. (d) Schematic diagram of the hysteresis loops of the top CoFeB layer showing the unipolar switching. (e) Schematic description of the switching process.[55,56]

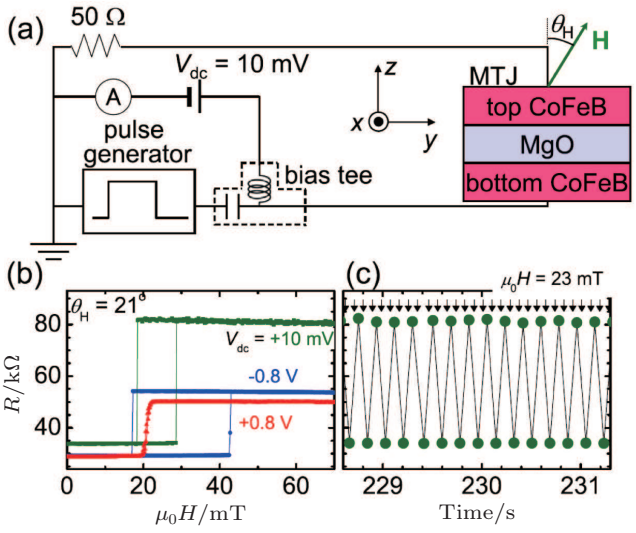


Fig. 13. (a) Schematic of experimental setup with PMA CoFeB/MgO/CoFeB MTJ. (b) Minor resistance versus magnetic field curves as a function of dc bias voltage. (c) Resistance measured after the application of voltage pulses of 0.9 V with 1.8 ns duration. Arrows indicate the time at which the voltage pulses are applied. The bias voltage pulse produces a temporal magnetic field.[57,58]

A similar magnetization reversal process was also obtained by Kanai *et al.* in PMA CoFeB/MgO/CoFeB MTJ system, utilizing nanosecond-duration unipolar bias voltage pulse under a static external magnetic field,[57] shown in Fig. 13. They mentioned that the temporal in-plane effective magnetic field can be produced by the bias voltage pulse with nanosecond duration through the change of magnetic anisotropy, and induce the precession of magnetization of the CoFeB free layer.

Almost at the same time, first-principles calculations showed that an external electric field can modify the PMA at the surface of ultrathin FM film.[59,60] It is known that the PMA at the oxide/FM interface is explained by the hybridization of the oxygen 2p orbital and Fe/Co 3d orbitals. Due to the degeneracy of 3d orbitals at the Fe/Co interface, the energy differs for the in-plane d orbitals (d_{xy}, $d_{x^2-y^2}$), and the out-of-plane d orbitals (d_{xz}, d_{yz}, and d_z^2). The magnetic anisotropy energy can be expressed in terms of the more-than-half-filled d orbital (Fe, Co)

$$\Delta U_{\mathrm{PMA}} = -\frac{G}{H}\frac{\xi}{4\mu_{\mathrm{B}}}(m_{\mathrm{orb}}^{\perp} - m_{\mathrm{orb}}^{\parallel}), \tag{6}$$

where G/H is a band structure-dependent coefficient, ξ is the orbital coupling constant, $m_{\mathrm{orb}}^{\perp}$ and $m_{\mathrm{orb}}^{\parallel}$ are the out-of-plane and the in-plane orbital moments, respectively. If $(m_{\mathrm{orb}}^{\perp} - m_{\mathrm{orb}}^{\parallel}) > 0$, the PMA is favorable. If $(m_{\mathrm{orb}}^{\perp} - m_{\mathrm{orb}}^{\parallel}) < 0$, the easy axis of magnetization is in-plane. When an electric field is applied at the oxide/FM interface, the redistribution of charge will induce changes between $m_{\mathrm{orb}}^{\perp}$ and $m_{\mathrm{orb}}^{\parallel}$.[61]

5. Summary

The progress of research into perpendicular magnetic materials, especially the CoFeB-MgO system with interfacial anisotropy, has pushed forward the development and the commercial applications of STT-MRAM toward a near-future goal of a sub-20 nm node. In addition, in ferromagnets where the magnetic properties are mainly dominated by the oxide/FM interface, large changes of magnetic anisotropy in response to applied electric field have been demonstrated. This effect can be used to achieve ultra-low-energy consumption MRAM, by reducing the switching energy barrier between the AP and P states of MTJs. Recently, a low switching current density of 10^4 A/cm^2 associated with a quasistatic unipolar voltage pulse, was obtained in CoFeB/MgO/CoFeB p-MTJ. Therefore, the perpendicular anisotropy materials have opened new possibilities in achieving high storage density, low-power operation and the third generation of MRAM.

References

[1] Tehrani S, Slaughter J M, Chen E, Durlam M, Shi J and DeHerrera M 1999 *IEEE Trans. Magn.* **35** 2814
[2] Tehrani S, Engel B, Slaughter J M, Chen E, DeHerrera M, Durlam M, Naji P, Whig R, Janesky J and Calder J 2000 *IEEE Trans. Magn.* **36** 2752
[3] Han X F, Wen Z C and Wei H X 2008 *J. Appl. Phys.* **103** 07E933
[4] Wang K L, Alzate J G and Amiri P K 2013 *J. Phys. D: Appl. Phys.* **46** 074003
[5] Chen E, Apalko D, Diao Z, Smith A D, Druist D, Lottis D, Nikitin V, Tang X, Watts S, Wang S, Wolf S A, Ghosh A W, Lu J W, Poon S J, Stan M, Butler W H, Gupta S, Mewes C K A, Mewes T and Visscher P B 2010 *IEEE Trans. Magn.* **46** 1873
[6] Han X F, Wen Z C, Wang Y, Liu H F, Wei H X and Liu D P 2011 *IEEE Trans. Magn.* **47** 2957
[7] Huai Y M 2008 *AAPPS Bulletin* **18** 33
[8] Slonczewski J C 1996 *J. Magn. Magn. Mater.* **159** L1
[9] Berger L 1996 *Phys. Rev. B* **54** 9353
[10] Katine J A, Albert F J, Buhrman R A, Myers E B and Ralph D C 2000 *Phys. Rev. Lett.* **84** 3149
[11] Huai Y M, Pakala M, Diao Z T, Apalkov D, Ding Y F and Panchula A 2006 *J. Magn. Magn. Mater.* **304** 88
[12] Wen Z C, Wei H X and Han X F 2007 *Appl. Phys. Lett.* **91** 122511
[13] Diao Z T, Apalkov D, Pakala M, Ding Y F, Panchula A and Huai Y M 2005 *Appl. Phys. Lett.* **87** 232502
[14] Tang D D and Lee Y J 2010 *Magnetic Memory Fundamentals and Technology* (New York: Cambridge University Press) p. 122
[15] Mangin S, Ravelosona D, Katine J A, Carey M J, Terris B D and Fullerton E E 2006 *Nat. Mater.* **5** 210
[16] Mangin S, Ravelosona D, Henry Y, Katine J A and Fullerton E E 2008 *AAPPS Bulletin* **18** 41
[17] Ohmori H, Hatori T and Nakagawa S 2008 *J. Appl. Phys.* **103** 07A911
[18] Kubota T, Ma Q L, Mizukami S, Zhang X M, Naganuma H, Oogane M, Ando Y and Miyazaki T 2013 *J. Phys. D: Appl. Phys.* **46** 155001
[19] Ma Q L, Kubota T, Mizukami S, Zhang X M, Naganuma H, Oogane M, Ando Y and Miyazaki T 2012 *Appl. Phys. Lett.* **101** 032402
[20] Yoshikawa M, Kitagawa E, Nagase T, Daibou T, Nagamine M, Nishiyama K, Kishi T and Yoda H 2008 *IEEE Trans. Magn.* **44** 2573
[21] Kim G, Sakuraba Y, Oogane M, Ando Y and Miyazaki T 2008 *Appl. Phys. Lett.* **92** 172502
[22] Park J H, Park C, Jeong T, Moneck M T, Nufer N T and Zhu J G 2008 *J. Appl. Phys.* **103** 07A917
[23] Tadisina Z R, Natarajarathinam A, Clark B D, Highsmith A L, Mewes T, Gupta S, Chen E and Wang S 2010 *J. Appl. Phys.* **107** 09C703
[24] You L, Sousa R C, Bandiera S, Rodmacq B and Dieny B 2012 *Appl. Phys. Lett.* **100** 172411
[25] Manchon A, Ducruet C, Lombard L, Auffret S, Rodmacq B, Dieny B, Pizzini S, Vogel J, Uhlí V, Hochstrasser M and Panaccione G 2008 *J. Appl. Phys.* **104** 043914
[26] Stöhr J and Siegmann H C 2006 *Magnetism: From Fundamentals to Nanoscale Dynamics* (New York: Springer) p. 504
[27] Tohnson M T, Bloemen P H, den Broeder F J A and de Vries J J 1996 *Rep. Prog. Phys.* **59** 1409
[28] Zhu L J, Nie S H, Meng K K, Pan D, Zhao J H and Zhen H Z 2012 *Adv. Mater.* **24** 4547
[29] Ma Q L, Kubota T, Mizukami S, Zhang X M, Naganuma H, Oogane M, Ando Y and Miyazaki T 2012 *Phys. Rev. B.* **87** 184426
[30] Monso S, Rodmacq B, Auffret S, Casali G, Fettar F, Gilles B, Dieny B and Boyer P 2002 *Appl. Phys. Lett.* **80** 4157
[31] Yang H X, Chshiev M, Dieny B, Lee J H, Manchon A and Shin K H 2011 *Phys. Rev. B.* **84** 054401
[32] Khoo K H, Wu G, Jhon M H, Tran M, Ernult F, Eason K, Choi H J and Gan C K 2013 *Phys. Rev. B* **87** 174403
[33] Khvalkovskiy A V, Apalkov D, Watts S, Chepulskii R, Beach R S, Ong A, Tang X, Smith A D, Butler W H, Visscher P B, Lottis D, Chen E, Nikitin V and Krounbi M 2013 *J. Phys. D: Appl. Phys.* **46** 074001
[34] Kryder M H, Gage E C, McDaniel T W, Challener W A, Rottmayer R E, Ju G P, Hsia Y T and Fatih E 2008 *Proc. IEEE* **96** 1810
[35] Nishimura N, Hirai T, Koganei A, Ikeda T, Okano K, Sekiguchi Y and Osada Y 2002 *J. Appl. Phys.* **91** 5246
[36] Cabrera A C, Chang C H, Hsu C C, Weng M C, Chen C C, Chao C T, Wu J C, Chang Y H and Wu T H 2007 *IEEE Trans. Magn.* **43** 914
[37] Nakayama M, Kai T, Shimomura N, Amano M, Kitagawa E, Nagase T, Yoshikawa M, Kishi T, Ikegawa S and Yoda H 2008 *J. Appl. Phys.* **103** 07A710
[38] Park J, Park C, Jeong T, Moneck M, Nuhfer N and Zhu J 2008 *J. Appl. Phys.* **103** 07A917
[39] Ye L X, Lee C M, Syu J W, Wang Y R, Lin K W, Chang Y H and Wu T H 2008 *IEEE Trans. Magn.* **44** 3601
[40] Yakushiji K, Noma K, Saruya T, Kubota H, Fukushima A, Nagahama T, Yuasa S and Ando K 2010 *Appl. Phys. Exp.* **3** 053003
[41] Mizunuma K, Yamanouchi M, Ikeda S, Sato H, Yamamoto H, Gan H D, Miura K, Hayakawa J, Matsukura F and Ohno H 2011 *Appl. Phys. Exp.* **4** 023002
[42] Mizunuma K, Ikeda S, Sato H, Yamanouchi M, Gan H D, Miura K, Yamamoto H, Hayakawa J, Matsukura F and Ohno H 2011 *J. Appl. Phys.* **109** 07C711
[43] Ikeda S, Miura K, Yamamoto H, Mizunuma K, Gan H D, Endo M, Kanai S, Hayakawa J, Matsukura F and Ohno H 2010 *Nat. Mater.* **9** 721
[44] Kim W, Jeong J H, Kim Y, Lim W C, Kim J H, Park J H, Shin H J, Park Y S, Kim K S, Park S H, Lee J E, Park S O, Choi S, Kang H K and Chung C 2011 *Tech. Dig. IEDM* **11** 531
[45] Wang W X, Yang Y, Naganuma H, Yu R C, Ando Y and Han X F 2011 *Appl. Phys. Lett.* **99** 012502
[46] Klein J, Leger A, Belin M and Defourneau D 1973 *Phys. Rev. B* **7** 2336
[47] Jang Y, Lee K, Lee S, Yoon S, Cho B K, Cho Y J, Kim K W and Kim K S 2009 *J. Appl. Phys.* **105** 07C901
[48] Wang S G, Ward R C C, Hesjedal T, Zhang X G, Wang C, Kohn A, Ma Q L, Zhang J, Liu F H and Han X F 2012 *J. Nanosci. Nanotechnol.* **12** 1006
[49] Anderson P W 1966 *Phys. Rev. Lett.* **17** 95
[50] Wei H X, Qin Q H, Ma Q L, Zhang X G and Han X F 2010 *Phys. Rev. B* **82** 134436
[51] Zhang S and Levy P M 1997 *Phys. Rev. Lett.* **79** 3744.
[52] Drewello V, Schäfers M, Schebaum O, Khan A A, Münchenberger J, Schmalhorst J, Reiss G and Thomas A 2009 *Phys. Rev. B* **79** 174417
[53] Weisheit M, Fähler S, Marty A, Souche Y, Poinsignon C and Givord D 2007 *Science* **315** 349
[54] Maruyama T, Shiota Y, Nozaki T, Ohta K, Toda N, Mizuguchi M, Tulapurkar A A, Shinjo T, Shiraishi M, Mizukami S, Ando Y and Suzuki Y 2009 *Nat. Nano.* **4** 158
[55] Wang W G, Li M, Hageman S and Chien C L 2012 *Nat. Mater.* **11** 64
[56] Wang W G and Chien C L 2013 *J. Phys. D: Appl. Phys.* **46** 074004
[57] Kanai S, Yamanouchi M, Ikeda S, Nakatani Y, Matsukura F and Ohno H 2012 *Appl. Phys. Lett.* **101** 122403
[58] Shiota Y, Nazaki T, Bonell F, Murakami S, Shinjo T and Suzuki Y 2012 *Nat. Mater.* **11** 39
[59] Shimabukuro R, Nakamura K, Akiyama T and Ito T 2010 *Physica E* **42** 1014
[60] Bruno P 1986 *Phys. Rev. B* **39** 865
[61] Niranjan M K, Duan C G, Jaswa S S and Tsymbal E Y 2010 *Appl. Phys. Lett.* **96** 222504